doi:10.1016/S0022-2836(02)01332-3 J. Mol. Biol. (2003) 326, 225–234

JMB

Available online at www.sciencedirect.com

SCIENCE DIRECT®

NMR Structure of a Variant Human Prion Protein with Two Disulfide Bridges

Ralph Zahn*, Peter Güntert, Christine von Schroetter and Kurt Wüthrich

Institut für Molekularbiologie und Biophysik, Eidgenössische Technische Hochschule Zürich CH-8093 Zurich, Switzerland

*Corresponding author

The nuclear magnetic resonance structure of the globular domain with residues 121–230 of a variant human prion protein with two disulfide bonds, hPrP(M166C/E221C), shows the same global fold as wild-type hPrP(121–230). It contains three α-helices of residues 144–154, 173–194 and 200–228, an anti-parallel β-sheet of residues 128–131 and 161–164, and the disulfides Cys166-Cys221 and Cys179-Cys214. The engineered extra disulfide bond in the presumed "protein X"-binding site is accommodated with slight, strictly localized conformational changes. High compatibility of hPrP with insertion of a second disulfide bridge in the protein X epitope was further substantiated by model calculations with additional variant structures. The ease with which the hPrP structure can accommodate a variety of locations for a second disulfide bond within the presumed protein X-binding epitope suggests a functional role for the extensive perturbation by a natural second disulfide bond of the corresponding region in the human doppel protein.

Keywords: prion protein; doppel protein; NMR structure; disulfide bonds; protein X epitope

Introduction

The three-dimensional structures of the human prion protein (hPrP) and the human doppel protein (hDpl) show a similar folding topology,[1,2] with a flexibly disordered N-terminal "tail" attached to a 100-residue globular C-terminal domain containing three α-helices and a small anti-parallel β-sheet. A striking difference between these two proteins concerns the number of disulfide bonds. In both hPrP and hDpl, a disulfide bridge linking the helices α2 and α3 is buried within the hydrophobic core, and contributes significantly to overall stability of the globular protein structure. It has been shown that reduction of the Cys residues 179 and 214 with dithiothreitol results in unfolding and aggregation of PrP *in vitro*,[3,4] implying that the so far unknown physiological functions of PrP, and presumably also Dpl, are dependent on this intact disulfide bond.

In Dpl, the loop between β-strand 2 and helix α2 is connected to a sequence position near the C terminus by an additional disulfide bond, which has no counterpart in wild-type PrP (Figure 1). The corresponding region of PrP with the residues 165–175 and 215–230 is devoid of cysteinyl residues. On the basis of inoculation studies with transgenic mice expressing various PrP constructs[5,6] this molecular region has been suggested to be an epitope for binding of a not yet further identified "protein X", which supposedly participates in the disease-related conformational transformation of PrP *in vivo*.[5,7–9]

The nuclear magnetic resonance (NMR) structures of the human and murine Dpl proteins show that the introduction of a second disulfide bond in the region corresponding to the presumed protein X-binding epitope in PrP (Figure 1) results in a

Present address: P. Güntert, RIKEN Genomic Sciences Center, W505, 1-7-22 Suehiro, Tsurumi, Yokohama 230-0045, Japan.

Abbreviations used: Dpl, doppel protein; hDpl, human Dpl; hPrP, human PrP; hPrP(121–230), recombinant fragment of hPrP comprising residues 121 to 230; hPrP(M166C/E221C), variant of hPrP(121–230) with Met166 and Glu221 substituted by Cys; hPrP(M166C/Y225C), variant of hPrP(121–230) with Met166 and Tyr225 substituted by Cys; NOE, nuclear Overhauser enhancement; NMR, nuclear magnetic resonance; $^{15}N\{^{1}H\}$-NOE, heteronuclear Overhauser enhancement of ^{15}N after saturation of ^{1}H; ppm, parts per million; PrP, prion protein.

E-mail address of the corresponding author: rz@mol.biol.ethz.ch

0022-2836/03/$ - see front matter

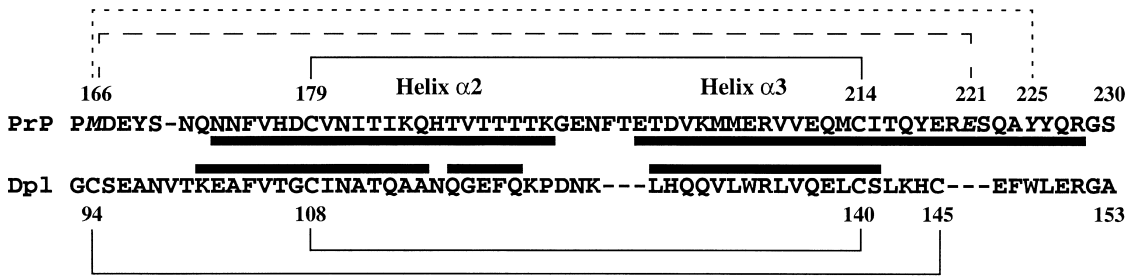

Figure 1. Amino acid sequence alignment of the human prion protein segment 165–230 and the human doppel protein segment 93–153 based on consideration of the sequences as well as the three-dimensional structures of the two proteins.[1,2] The residue positions in hPrP that were exchanged against Cys in this paper are in italics. Continuous black lines indicate the natural disulfide bridges, and the locations of the regular α-helical secondary structures in the wild-type proteins are indicated by black boxes. The broken and dotted lines indicate, respectively, the extra disulfide bond in hPrP(M166C/E221C), for which a complete structure was obtained, and in hPrP(M166C/Y225C), which was also expressed and characterized.

major change of the three-dimensional structure. To investigate the effect of an artificial extra disulfide bond in this region of the three-dimensional prion protein structure we generated two variants of the globular domain of the human prion protein, hPrP(121–230). hPrP(M166C/E221C) and hPrP (M166C/Y225C) were designed so as to simultaneously mimic the location of the second disulfide bond in hDpl (Figure 1) and to be compatible with the three-dimensional structure of wild-type human PrP.[2] Among the sites thus chosen for the amino acid substitutions in hPrP, Glu221 is fully conserved in the amino acid sequences of 27 mammalian and nine avian prion proteins,[10] Tyr225 is replaced with Ser, Phe or Ala in some of the species, and Val166 is replaced by Met or Ile only in human, chimpanzee and marsupial PrP. Among the known Dpl sequences,[11] the residues Cys94 and Cys145 in the second disulfide bond are fully conserved.

Here, we describe a high-quality NMR structure of hPrP(M166C/E221C), a qualitative spectroscopic characterization of hPrP(M166C/Y225C), and model calculations of additional two-disulfide variants of hPrP(121–230). The results are evaluated with regard to possible functional roles of the protein X-binding epitope in PrP and the corresponding molecular region in Dpl.

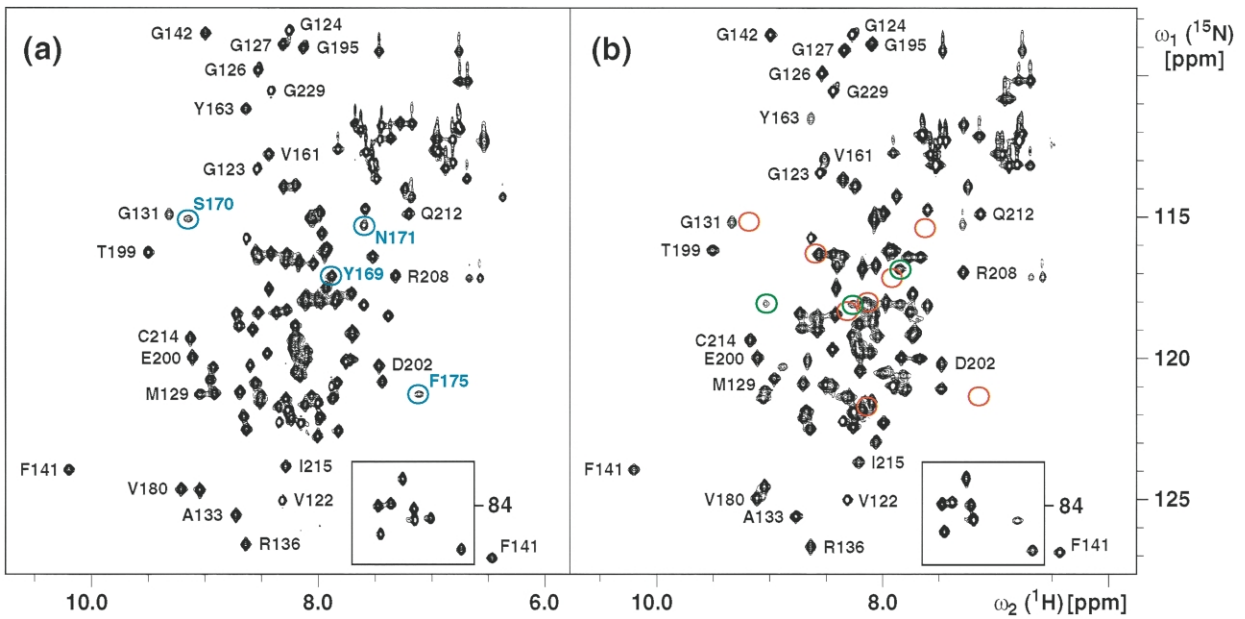

Figure 2. Two-dimensional [^{15}N,^{1}H]-correlation spectroscopy (COSY) spectra of (a) hPrP(M166C/E221C) and (b) hPrP(M166C/Y225C). Selected cross-peak assignments are indicated with black lettering. In (a), blue circles and blue lettering indicate cross-peaks that have been observed for hPrP(M166C/E221C), but have not been seen either in the spectra of hPrP(M166C/Y225C) or wild-type hPrP(121–230).[2] In (b), empty red circles identify positions where cross-peaks were expected from comparison with (a) and with hPrP(121–230), and green circles indicate cross-speaks that could not be assigned because of missing sequential connectivities in the triple-resonance spectra. In both spectra the rectangular frame encloses folded cross-peaks of $H^{N\varepsilon}$ in Arg side-chains. The spectra were recorded at 600 MHz with 1 mM protein solutions in 90% H_2O/10% ^2H_2O, 10 mM [d_4]-sodium acetate at pH 4.5 and $T = 20$ °C.

Table 1. Characterization of the 20 energy-refined DYANA conformers representing the NMR structure of hPrP(M166C/E221C)

Quantity	Value[a]
Residual DYANA target function value (Å^2)[b]	1.05 ± 0.13
Residual NOE distance constraint violations	
Number > 0.1 Å	32 ± 5
Maximum (Å)	0.14 ± 0.01
Residual dihedral angle constraint violations	
Number > 2.5 degrees	0 ± 0
Maximum (degrees)	1.64 ± 0.41
Residual disulfide bond constraint violations	
Number > 0.1 Å	0 ± 0
Maximum (Å)	0.02 ± 0.02
AMBER energy (kcal/mol)	
Total	−4641 ± 92
van der Waals	−293 ± 14
Electrostatic	−5285 ± 78
RMSD from ideal geometry	
Bond lengths (Å)	0.0078 ± 0.0002
Bond angles (degrees)	1.91 ± 0.04
RMSD, N, C$^\alpha$, C′ (125–228) (Å)[c]	0.63 ± 0.13
RMSD, all heavy atoms (125–228) (Å)[c]	1.11 ± 0.11

The input consisted of 1775 NOE upper distance constraints, 116 dihedral angle constraints on ϕ and ψ, and six upper distance and six lower distance constraints to enforce the disulfide bonds 166–221 and 179–214.

[a] Average values ± standard deviations for the 20 energy-minimized conformers with the lowest DYANA target function values are given.

[b] Before energy minimization.

[c] RMSD values relative to the mean coordinates.

Results

Production and spectroscopic characterization of two variant prion proteins

The two variant proteins hPrP(M166C/E221C) and hPrP(M166C/Y225C) were expressed as inclusion bodies in *Escherichia coli* and purified by high-affinity column refolding, which resulted in a similar yield to wild-type hPrP(121–230).[2,12] The formation of an additional disulfide bond was confirmed by mass spectrometry, and resulted in an increase of the melting temperature by about 10 °C for both proteins (data not shown). The variant proteins were uniformly ^{13}C,^{15}N-labeled for resonance assignment and structure determination. Solutions containing 1 mM protein and 10 mM sodium acetate at pH 4.5 and 20 °C were used for the NMR experiments.

The ^{1}H NMR spectra of both proteins showed that the preparations are homogeneous, and the chemical shift dispersion is typical for globular proteins. Closely similar structures are clearly apparent by the chemical shifts observed by two-dimensional [^{15}N,^{1}H]-correlation spectroscopy (COSY) (Figure 2). However, whereas in the spectrum of hPrP(M166C/E221C) (Figure 2(a)) all 108 expected backbone amide resonances were observed (the thrombin cleavage site adds a Gly-Ser dipeptide preceding the N terminus of the prion protein sequence,[12] so that the resonances of Ser120 and Val121 are also observed in the [^{15}N,^{1}H]-COSY spectrum), we could identify only 103 backbone amide resonances in hPrP(M166C/Y225C) (Figure 2(b)). Throughout, the resonance lines of the amide protons in hPrP(M166C/Y225C) are broadened by about 6 Hz in comparison with spectrum A, which indicates transient aggregation of this variant protein into oligomers.

Resonance assignment and structure determination of hPrP(M166C/E221C)

Sequence-specific backbone assignments were obtained using standard triple-resonance experiments with the ^{13}C,^{15}N-labeled protein,[13] and the sequence-specific assignments were independently confirmed by sequential and medium-range nuclear Overhauser enhancement (NOE) cross-peaks.[14] All polypeptide backbone resonances were assigned, including the amide nitrogen atoms and amide protons of all the residues in the loop 165–172 and of Phe175 (Figure 2(a)), which were not detected in the wild-type protein.[2] At least either one heteronuclear sequential scalar connectivity or a sequential NOE has been observed for each pair of neighboring residues. The side-chains were assigned based on chemical shift comparison with wild-type hPrP(121–230),[2] and have been confirmed using a three-dimensional ^{15}N-resolved [^{1}H,^{1}H]-total correlation spectroscopy (TOCSY) spectrum.[15] The side-chain assignments of non-labile protons are complete, with the sole exceptions of εCH of His155 and His187, and ζCH of Phe175 and Phe198. Among the labile side-chain protons, the amide groups of all seven Asn and Gln residues and the ε-proton resonances of the eight Arg residues were assigned by intraresidual NOEs.[14] Of the side-chain hydroxyl protons of Ser, Thr and Tyr only the resonance of Thr183 could be observed and assigned.

The methyl groups of the nine Val and two Leu residues in hPrP(M166C/E221C) were stereospecifically assigned, and additional stereospecific assignments were obtained for two αCH_2, 30 βCH_2, 17 γCH_2 and four δCH_2 groups, using the program FOUND[16] implemented in the DYANA package.[17] The $^{13}C^\beta$ resonances of the four Cys residues are all strongly downfield-shifted in the range 39.6–41.6 ppm, confirming that they all form disulfide bonds.[18]

A total of 4477 nuclear Overhauser enhancement spectroscopy (NOESY) cross-peaks were interactively picked and integrated in a 750 MHz three-dimensional combined ^{15}N/^{13}C-resolved [^{1}H,^{1}H]-NOESY spectrum recorded in H_2O with a mixing time of 40 ms. Using the two peak lists for NOEs with at least one ^{15}N-bound and at least one ^{13}C-bound proton, respectively, and the chemical shift list as input for the programs CANDID for automated NOE assignment[19] and DYANA for structure calculation[17] (see Materials and Methods for

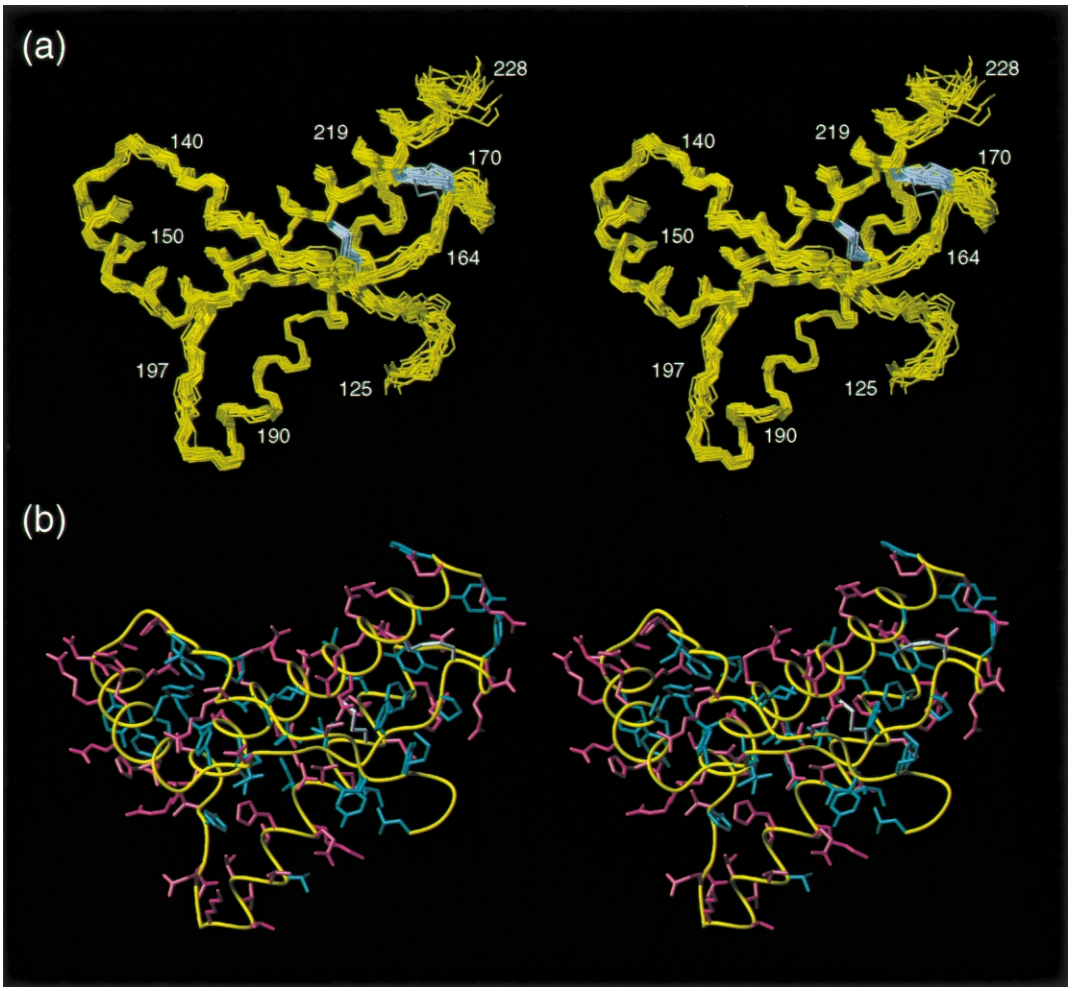

Figure 3. Stereo views of the NMR structure of hPrP(M166C/E221C). (a) Backbone of 20 energy-refined DYANA conformers superimposed for best fit of the N, C^{α} and C′ atoms of residues 125–228. (b) All-heavy-atom representation of the conformer from (a) with the smallest deviation from the mean coordinates. The backbone is shown as a yellow spline function through the C^{α} positions, hydrophobic side-chains are cyan, and polar and charged side-chains are pink. In both drawings the two disulfide bridges are drawn in white.

details), 1775 NOE upper limit distance constraints were obtained. As supplementary conformational constraints, all residues with $^{13}C^{\alpha}$ chemical shifts deviating from the random coil values by more than 1.5 ppm were subjected to the following bounds on the dihedral torsion angles: $-120° < \Phi < -20°$ and $-100° < \Psi < °$ for deviations >1.5 ppm; $-200° < \Phi < -80°$ and $40° < \Psi < 220°$ for deviations < -1.5 ppm.[20] The combined information from the intraresidual and sequential NOEs, and the $^{13}C^{\alpha}$ chemical shifts used as input for the program FOUND yielded 458 constraints on dihedral angles ϕ, ψ, χ^1 and χ^2. Three upper and three lower distance limits were used to enforce each of the two disulfide bonds Cys166-Cys221 and Cys179-Cys214.[21] The final DYANA calculation in the seventh cycle of the CANDID standard protocol[19] was performed with 100 randomized starting structures, and the 20 best DYANA conformers were further energy-refined with the program OPALp.[22,23] The resulting bundle of 20 energy-minimized conformers is used to represent the NMR structure. Table 1 gives a survey of the results of the structure calculation. The small residual constraint violations show that the structure is consistent with the experimental constraints, and the global RMSD values among the bundle of 20 conformers are representative of a high-quality structure determination (Figure 3).

New calculation of the wild-type hPrP(121–230) NMR structure with the programs CANDID and DYANA

Given that the main interest of this paper is focused on comparison of variant human prion proteins with wild-type hPrP(121–230), we re-evaluated the NOE input data and repeated the structure calculation of the previously published hPrP(121–230) structure[2] with the new CANDID/DYANA protocol.[19] This ensures that the structure comparisons in this paper are not influenced by systematic differences that might arise from the use of somewhat different protocols for data

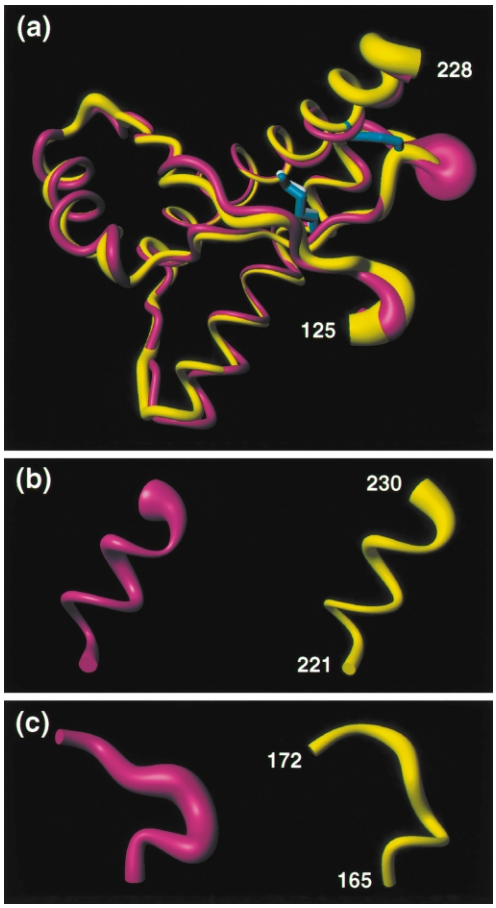

Figure 4. Comparison of the mean NMR structures of hPrP(M166C/E221C) (yellow) and hPrP(121–230) (magenta). (a) Residues 125–228. (b) Residues 221–230. (c) Residues 165–172. In this presentation, a spline function was drawn through the C^{α} positions, and the radius of the cylindrical rods was adjusted proportional to the mean global backbone displacement per residue among the 20 energy-minimized conformers used to represent the solution structure.[40] The relative orientations of the two molecules resulted from a superposition for best fit of the backbone heavy atoms in the segment bounded by the sequence positions indicated in the Figure. In (a) the disulfide bridges in hPrP(M166C/E221C) and wild-type hPrP(121–230) are drawn in cyan and white, respectively.

analysis and calculation of the new structures of variant proteins and the reference wild-type structure.

Influence of the additional disulfide bond on conformational equilibria in the NMR structure of hPrP(M166C/E221C)

The NMR structure of hPrP(M166C/E221C) has the same global fold as hPrP(121–230), with an RMSD value of 1.08 Å between the backbone heavy atoms of residues 125–228 in the mean structures of the two proteins (Figure 4(a)). Regular secondary structures include a short two-stranded anti-parallel β-sheet with residues 128–131 and 161–164, helix α1 with residues 144–154, helix α2 with residues 173–194, and helix α3 with residues 200–228.

Within the framework of the preserved global structure, there are variations in the precision of the structure determination for loop 165–172 in the variant and wild-type hPrP(121–230). In the wild-type protein, the backbone amide resonances of three amino acid residues in the loop 165–172 are not observable, presumably because of line broadening attributable to slow conformational exchange on the NMR chemical shift time scale.[2] This results in reduced precision of the structure determination for the segment 165–172, because of scarcity of NOE upper distance limit constraints. In contrast, complete polypeptide backbone assignments were obtained for hPrP(M166C/E221C), which enabled the identification of additional medium-range NOEs in the loop 165–172, which is therefore significantly better defined than in the wild-type protein (Figure 4(c)). The disulfide bond between Cys166 and Cys221 thus seems to reduce the conformation space accessible to the loop 165–172 and thus to largely suppress the previously observed exchange broadening of backbone amide resonances in this polypeptide segment.[2]

The helix α3 is equally well defined in hPrP(M166C/E221C) and hPrP(121–230) (Figure 4(b)), and differences between the two structures are within the conformation space spanned by the bundles of 20 conformers (Figure 4(a)). These observations in the calculated structures correlate with near-identical density of NOE distance constraints, in particular medium-range constraints $d_{\alpha N}(i, i+3)$, $d_{\alpha N}(i, i+4)$ and $d_{\alpha\beta}(i, i+3)$, which have a dominant influence on the regular α-helix fold.[14] Because of the dependence of the NOE intensity on the inverse sixth power of the distance d, only folded forms of a polypeptide with short d values contribute significantly to the observed NOEs, so that in the presence of rapid conformational equilibria with unfolded forms only the folded structure is usually obtained in a NOE-based NMR structure determination. Different averaging applies to the differences between observed and random coil $^{13}C^{\alpha}$ chemical shifts, $\Delta\delta(^{13}C^{\alpha})$, which can therefore be qualitatively related to the populations of regular secondary structures.[20,24–26] Figure 5(a) shows that although for all $^{13}C^{\alpha}$ atoms located within helix α3 of hPrP(M166C/E221C) the resonances are shifted downfield relative to the random coil shifts, the smaller values of $\Delta\delta(^{13}C^{\alpha})$, for all residues in the C-terminal two turns indicate lower population of the α-helical structure towards the C terminus. Considering that it appears not to be manifested in the NOE-based structure (Figure 4(a) and (b)), this equilibrium seems to be with unfolded forms of the polypeptide. Comparing the values of $\Delta\delta(^{13}C^{\alpha})$, between hPrP(M166C/E221C) and hPrP(121–230) further shows that all but one of the chemical shifts within the segment 222–228 of the variant protein are shifted upfield (Figure

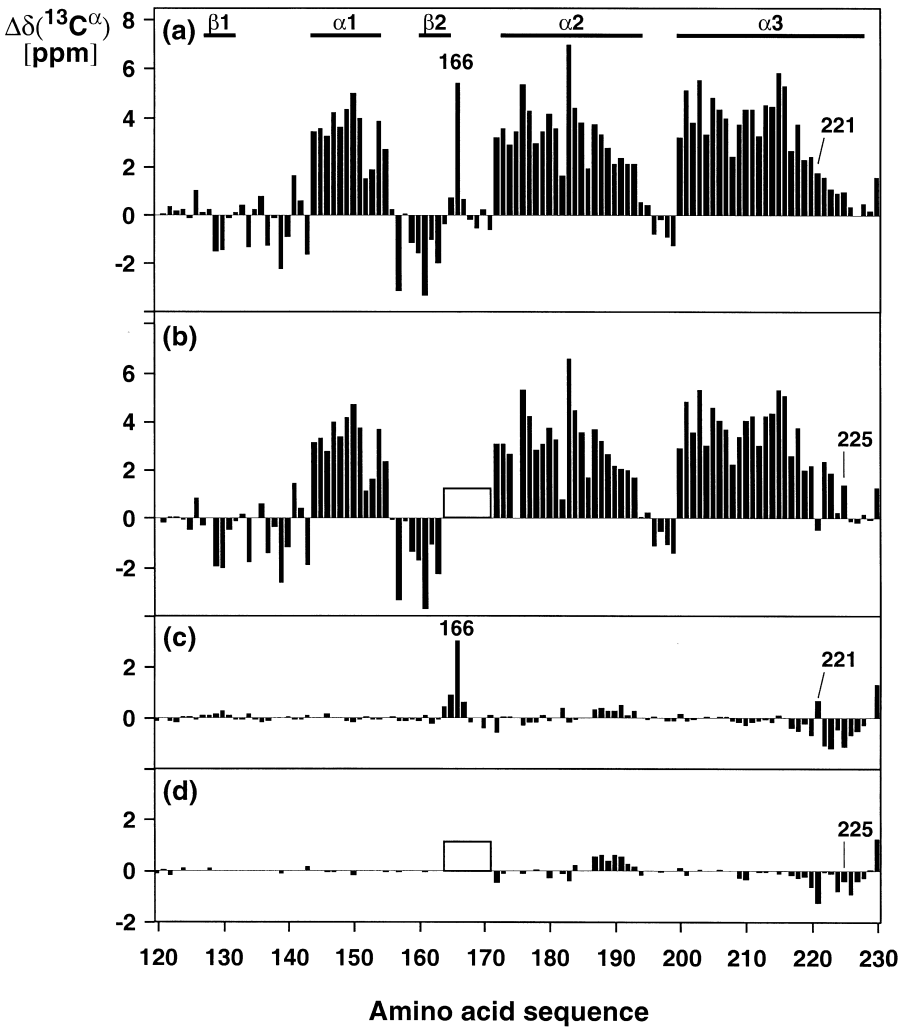

Figure 5. Plots *versus* the hPrP(121–230) amino acid sequence of $^{13}C^{\alpha}$ chemical shift differences, $\Delta\delta(^{13}C^{\alpha})$. (a) and (b), hPrP(M166C/E221C) and hPrP(M166C/Y225C), respectively, *versus* the random coil shifts;[18,41] (c) and (d), hPrP(M166C/E221C) and hPrP(M166C/Y225C), respectively, *versus* wild-type hPrP(121–230).[2] The positions of the amino acid replacements in the two variants of hPrP(121–230) are indicated by the sequence positions. The rectangle in (b) and (d) indicates the residues 164–171, for which the $^{13}C^{\alpha}$ chemical shifts could not be assigned in hPrP(M166C/Y225C). In (c) and (d), no data are given for residues 169 and 175, since these $^{13}C^{\alpha}$ chemical shifts could not be assigned in hPrP(121–230). The locations of the regular secondary structure elements are given at the top.

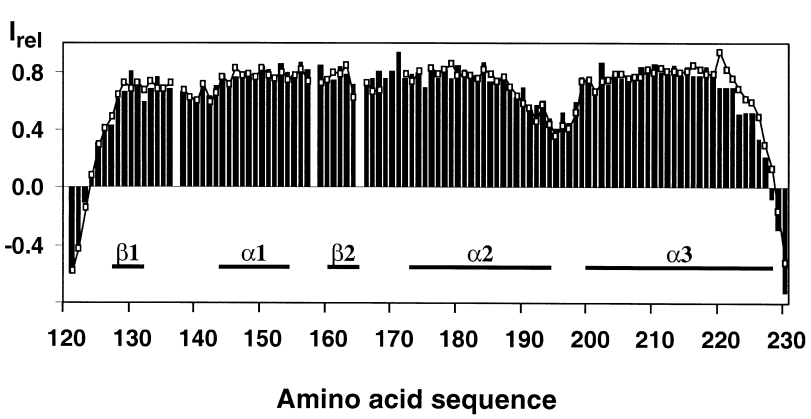

Figure 6. Steady-state $^{15}N\{^{1}H\}$-NOEs of hPrP(M166C/E221C) (black bars) and hPrP(121–230) (open squares). For hPrP(121–230), the amide protons of residues 169, 170, 171 and 175 could not be observed because of line broadening. Residues 137, 158 and 165 are proline. The locations of the regular secondary structure elements are indicated at the bottom.

Table 2. Characterization of two-disulfide variants of hPrP(121–230) calculated after adding constraints for the introduction of an extra disulfide bond to the input used previously for the structure determination of wild-type hPrP(121–230)

Disulfide bond constraints	NOEs[a]	Target function[b]	Violations[c]	RMSD[d]	$\overline{\text{RMSD}}$[e]
179–214 (wild-type)	1798	0.74 ± 0.07	0 ± 0	0.65 ± 0.10	
166–221, 179–214	1767	0.73 ± 0.07	0 ± 0	0.62 ± 0.12	0.54
166–225, 179–214	1767	0.76 ± 0.08	0 ± 0	0.72 ± 0.11	0.47
165–221, 179–214	1777	0.78 ± 0.08	0 ± 0	0.67 ± 0.13	0.26
165–222, 179–214	1780	1.09 ± 0.15	0 ± 0	0.66 ± 0.12	0.66
165–225, 179–214	1776	0.84 ± 0.10	0 ± 0	0.71 ± 0.09	0.99
166–222, 179–214	1770	0.80 ± 0.08	0 ± 0	0.65 ± 0.16	0.42
166–179, 214–221	1767	23.1 ± 0.40	4 ± 1	0.80 ± 0.12	3.47
166–214, 179–221	1767	14.8 ± 0.45	5 ± 0	0.83 ± 0.23	3.58

Eight different variant proteins were generated by combination of the two natural Cys residues and two artificial extra Cys residues into two disulfide bonds, where the extra cysteine residues occupy five different sequence positions. The input for the structure calculations was adapted from the input for wild-type hPrP(121–230) (see Figure 4), the data of which are also listed in the top row for comparison. For the two Xxx-to-Cys exchanges, NOEs with side-chain protons beyond βCH_2 were eliminated from the NOE upper distance constraints listed in the second column. Each of the disulfide bonds listed in the first column was enforced by the standard three upper and three lower distance constraints.[21] Each calculation was started with 100 randomized structures.

[a] Number of NOE upper distance constraints in the input.

[b] Residual DYANA target function value (Å^2). The average ± standard deviation is given for a bundle of 20 conformers used to represent the structure.

[c] Average number ± standard deviation of residual upper limit disulfide bond constraint violations larger than 0.1 Å. The number of residual lower limit disulfide bond constraint violations >0.1 Å was in all calculations between 0 and 1.

[d] RMSD value (Å, average ± standard deviation) of the bundle of 20 conformers relative to the mean coordinates calculated for the backbone heavy atoms N, C^α and C′ of residues 125–228.

[e] RMSD value (Å) between the mean structures of the variant protein and hPrP(121–230) calculated for residues 125–228.

5(c)). The introduction of the additional disulfide bond thus seems to slightly decrease the population of helical structure in the C-terminal two turns of α3.

The conformational equilibria manifested in the $^{13}C^\alpha$ chemical shifts correlate with intramolecular rate processes that may be detected by measurement of heteronuclear $^{15}N\{^1H\}$-NOEs. For hPrP(121–230) and hPrP(M166C/E221C) the $^{15}N\{^1H\}$-NOEs show a uniform distribution over most of the amino acid sequence, with typical values for a globular protein with the size of hPrP(121–230) (Figure 6). Besides the last two turns of helix α3, only the residues 121–126, which are unstructured and connect the globular domain with the flexible tail in the intact PrP, and the residues 191–198, which form the somewhat disordered C-terminal end of helix α2 and the subsequent loop,[2] show decreased positive or negative $^{15}N\{^1H\}$-NOE values. In both proteins the helix α3 is thus the only well-defined structural region with somewhat higher-than-average internal mobility, and the introduction of the extra disulfide bond in hPrP(M166C/E221C) causes both a lowering of the population of the α3 helix structure and a slight increase of its internal mobility.

Spectroscopic characterization of hPrP(M166C/Y225C)

The increased linewidths in the NMR spectra of hPrP(M166C/Y225C) (Figure 2(b)) precluded complete backbone assignments. No unambiguous assignments could be obtained for the amide protons and amide nitrogen atoms of Arg164, Cys166, Asp167, Glu168, Tyr169, Ser170, Asn171 and Phe175. In view of both the limited quality of the NMR data and the results of the model calculations described below, we only completed a $^{13}C^\alpha$ chemical shift-based analysis of regular secondary structure. As a result, the $^{13}C^\alpha$ chemical shift differences relative to the random coil shifts (Figure 5(b)) as well as relative to wild-type hPrP(121–230) (Figure 5(d)) show that the secondary structure elements of the wild-type hPrP(121–230) are conserved also for this variant protein.

Model calculations for additional hPrP(121–230) variants with two disulfide bonds

To investigate the compatibility of the wild-type hPrP(121–230) structure with alternative positioning of an extra disulfide bridge, we used the program DYANA[17] for a series of model calculations. As an input for these calculations we used the same distance and dihedral angle constraints as for the aforementioned new structure determination of hPrP(121–230), except that three upper and three lower distance limits were added to enforce each one of the different individual extra disulfide bonds,[21] and all NOE constraints with protons beyond βCH_2 of the residues that were replaced by cysteine were eliminated. The results in Table 2 show that all the calculations with disulfide constraints linking residues 165 or 166 with any of the residues 221, 222 or 225 converged well, with no or only a slight increase of the residual DYANA target function value when compared to the calculation for hPrP(121–230). Furthermore, the introduction of these disulfide bonds did in no case lead to significant residual upper limit disulfide constraint violations, and the

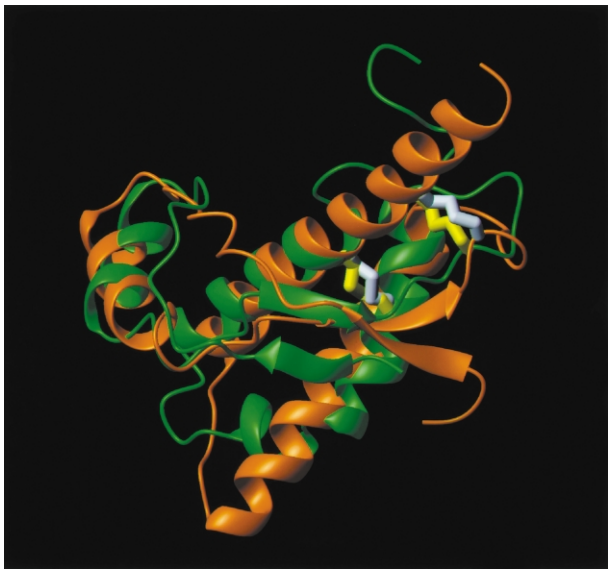

Figure 7. Comparison of the three-dimensional structures of hPrP(M166C/E221C) and hDpl(24–152) (the drawing was prepared from the atom coordinates deposited in the Protein Data Bank, accession code 1LG4).[1] The hPrP(M166C/E221C) molecule has approximately the same orientation as in Figure 3. The superposition of the two molecules is for best fit of the backbone atoms of the helical polypeptide segments 146–152, 173–186 and 201–215 in hPrP(M166C/E221C) with 74–80, 102–115 and 127–141 in hDpl. The following color code was used: orange and white, polypeptide backbone (residues 125–230) and disulfide bridges of hPrP(M166C/E221C), respectively; green and yellow, backbone (residues 56–152) and disulfide bridges of hDpl, respectively.

root-mean-square deviation of the variant protein relative to the mean coordinates of hPrP(121–230) (RMSD) was within the conformation space spanned by the 20 conformers. As an internal control we also investigated proteins with disulfide bonds linking one of the wild-type Cys residues with one of the artificial Cys residues. These calculations resulted in structures with extensively increased residual target function values, disulfide bond constraint violations, and RMSD values.

Discussion

Comparison of the globular domains of human Dpl and human PrP reveals both close global similarities and marked local differences.[1] Similar observations were reported for the corresponding murine proteins.[27] Figure 7 illustrates the following differences between the hPrP and hDpl structures: within the region of the hDpl structure that corresponds to the presumed protein X epitope in hPrP,[5,8] the helix α3 is shortened by more than two turns, and the C-terminal peptide segment 144–149 is folded against the loop connecting β2 and α2. Between the two proteins, the plane of the β-sheet, which immediately precedes the protein X epitope in the PrP sequence, is rotated by about 180° with respect to the molecular scaffold formed by the helical secondary structures, and in hDpl it is located two residues closer to the helix α1. Furthermore, in hDpl the helix α2 of hPrP, which follows the protein X epitope in the PrP sequence, is replaced by two shorter helices $\alpha 2^a$ and $\alpha 2^b$. The present structure determination of a variant human prion protein containing two disulfide bonds now enables novel insights into the relations between the molecular structures of hPrP and hDpl in the region of the protein X epitope, which may also support the ongoing search for the still unknown functions of the two proteins.

The global structure of the variant hPrP is similar to both wild-type hPrP (Figure 4) and hDpl (Figure 7). The RMSD value between the backbone heavy atoms of residues involved in the common α-helices of the mean structures of hPrP(M166C/E221C) and hDpl is 1.69 Å. After superposition of the three-dimensional structures for minimal RMSD of this scaffold (Figure 7), the positions and orientations of the artificial disulfide bond in hPrP(M166C/E221C) and of the corresponding natural disulfide bond in hDpl are closely similar. This is rather surprising, considering that in hDpl the disulfide bond Cys94-Cys145 connects two segments without regular secondary structure, i.e. the loop 91–100 and the C-terminal segment of residues 142–153, whereas in the variant hPrP the disulfide Cys166-Cys221 anchors the mobile loop 165–172 against the helix α3 (see Figures 1 and 7). From the present data it appears plausible that the local structure of the presumed protein X epitope observed in PrP might initially also have been present in Dpl, with a cysteinyl residue at position 94 forming a disulfide bond with a second cysteinyl located in a position that would have been compatible with the helix α3 extending all the way to the C terminus, e.g. position 147 (Figure 1). During further evolution, a deletion in helix α3 could have relocated this cysteinyl into position 145 (Figure 1), where it is incompatible with regular α-helix structure beyond about residue 141. Nature would then appear to have selected for this disulfide bridge and the poorly structured C-terminal peptide segment. Since this disulfide bond is common to all known mammalian Dpl sequences,[11] there is a clear indication that this intriguing choice of the Cys position nearest to the C terminus has a specific role in the physiological Dpl function. A different function of this structural region of Dpl from that of the protein X epitope in PrP is independently suggested by the fact that the loop 91–100 contains an Asn-linked glycosylation site at position 98,[11] which has no counterpart in PrP. If protein X interactions are indeed essential for prion propagation, then the disulfide-related different conformation in this molecular region of Dpl may provide a rationale for the observation that no Dpl is found in preparations of prions[28] and no evidence could so far be obtained for a TSE that would be caused by Dpl.[29,30] In fact, the second disulfide bond in Dpl may have evolved to prevent a conformational transition into a pathogenic form by precluding an interaction with protein X.

Materials and Methods

Sample preparation and characterization

For the cloning, expression and purification of the two-disulfide hPrP(121–230) variants in unlabeled form and with uniform ^{13}C,^{15}N-labeling we closely followed the strategy used for the preparation of wild-type hPrP,[2,12] where double-residue exchanges were constructed following the Quickchange site-directed mutagenesis protocol (Stratagene). Protein solutions of 1 mM in 90% H_2O/10% ^2H_2O containing 10 mM [d_4]-sodium acetate at pH 4.5 for NMR spectroscopy were obtained using Ultrafree-15 Centrifugal Filter Biomax Devices (Millipore).

NMR measurements and structure calculations

The NMR measurements were performed on Bruker DRX500, DRX600 and DRX750 spectrometers equipped with four radio-frequency channels and triple resonance probeheads with shielded *z*-gradient coils. For the collection of conformational constraints, a three-dimensional combined $^{15}N/^{13}C$-resolved [^1H,^1H]-NOESY spectrum[31,32] in H_2O was recorded with a mixing time $\tau_m = 40$ ms at $T = 20$ °C, $256(t_1) \times 50(t_2) \times 1024(t_3)$ complex points, $t_{1,max}(^1H) = 28.4$ ms, $t_{2,max}(^{15}N) = 20.6$ ms, $t_{2,max}(^{13}C) = 8.3$ ms, $t_{3,max}(^1H) = 97.5$ ms, and this data set was zero-filled to $512 \times 128 \times 2048$ points. Processing of the spectra was performed with the program PROSA.[33] The ^1H, ^{15}N and ^{13}C chemical shifts have been calibrated relative to 2,2-dimethyl-2-silapentane-5-sulfonate, sodium salt.

Steady-state $^{15}N\{^1H\}$-NOEs were measured at 600 MHz following the method described.[34] using a proton saturation period of five seconds by applying a cascade of 120° pulses in 20 ms intervals; $t_{1,max}(^{15}N) = 61.0$ ms, $t_{2,max}(^1H) = 142.6$ ms, time domain data size 152×1024 complex points.

NOE assignment was obtained using the CANDID software[19] in combination with the structure calculation program DYANA.[17] CANDID and DYANA perform automated NOE-assignment and distance calibration of NOE intensities, removal of covalently fixed distance constraints, structure calculation with torsion angle dynamics, and automatic NOE upper distance limit violation analysis. As input for CANDID, peak lists of the aforementioned NOESY spectrum were generated by interactive peak picking with the program XEASY[35] and automatic integration of the peak volumes with the program SPSCAN (Ralf Glaser, personal communication). The input for the calculations with CANDID and DYANA contained these peak lists, a chemical shift list from the previous sequence-specific resonance assignment, and dihedral angle constraints for the backbone angles ϕ and ψ that were derived from $^{13}C^{\alpha}$ shifts.[20] The calculation followed the standard protocol of seven cycles of iterative NOE assignment and structure calculation.[19] During the first six CANDID cycles, ambiguous distance constraints[36] were used. For the final structure calculation, only NOE distance constraints were retained that correspond to NOE cross-peaks with unambiguous assignment after the sixth cycle of calculation. Stereospecific assignments were identified by comparison of upper distance limits with the structure resulting from the sixth CANDID cycle.[37] The 20 conformers with the lowest final DYANA target function values were energy-minimized in a water shell with the program OPALp,[22,23] using the AMBER force field.[38] The program MOLMOL[39] was used to analyze the resulting 20 energy-minimized conformers (Tables 1 and 2) and to prepare drawings of the structures.

Atomic coordinates

The atomic coordinates of the bundle of 20 conformers have been deposited with the Protein Data Bank, accession code 1H0L. The ^1H, ^{13}C and ^{15}N chemical shifts for hPrP(M166C/ E221C) have been deposited with the Biological Magnetic Resonance Bank, file 5378.

Acknowledgements

Financial support was obtained from the Schweizerischer Nationalfonds (projects 31.49047.96 and 438 + 050287).

References

1. Lührs, T., Riek, R., Güntert, P. & Wüthrich, K. (2003). *NMR structure of the human doppel protein*, In press.
2. Zahn, R., Liu, A., Lührs, T., Riek, R., von Schroetter, C., López García, F. *et al.* (2000). NMR solution structure of the human prion protein. *Proc. Natl Acad. Sci. USA*, **97**, 145–150.
3. Mehlhorn, I., Groth, D., Stöckel, J., Moffat, B., Reilly, D., Yansura, D. *et al.* (1996). High-level expression and characterization of a purified 142-residue polypeptide of the prion protein. *Biochemistry*, **35**, 5528–5537.
4. Jackson, G. S., Hosszu, L. L., Power, A., Hill, A. F., Kenney, J., Saibil, H. *et al.* (1999). Reversible conversion of monomeric human prion protein between native and fibrilogenic conformations. *Science*, **283**, 1935–1937.
5. Telling, G. C., Scott, M., Hsiao, K. K., Foster, D., Yang, S., Torchia, M. *et al.* (1994). Transmission of Creutzfeldt-Jakob disease from humans to transgenic mice expressing chimeric human-mouse prion protein. *Proc. Natl Acad. Sci. USA*, **91**, 9936–9940.
6. Telling, G. C., Scott, M., Mastrianni, J., Gabizon, R., Torchia, M., Cohen, F. E. *et al.* (1995). Prion propagation in mice expressing human and chimeric PrP transgenes implicates the interaction of cellular PrP with another protein. *Cell*, **83**, 79–90.
7. Billeter, M., Riek, R., Wider, G., Hornemann, S., Glockshuber, R. & Wüthrich, K. (1997). Prion protein NMR structure and species barrier for prion diseases. *Proc. Natl Acad. Sci. USA*, **94**, 7281–7285.
8. Prusiner, S. B. (1998). Prions. *Proc. Natl Acad. Sci. USA*, **95**, 13363–13383.
9. Zahn, R. (1999). Prion propagation and molecular chaperones. *Q. Rev. Biophys.* **32**, 309–370.
10. Wopfner, F., Weidenhofer, G., Schneider, R., von Brunn, A., Gilch, S., Schwarz, T. F. *et al.* (1999). Analysis of 27 mammalian and 9 avian PrPs reveals high conservation of flexible regions of the prion protein. *J. Mol. Biol.* **289**, 1163–1178.
11. Moore, R. C., Lee, I. Y., Silverman, G. L., Harrison, P. M., Strome, R., Heinrich, C. *et al.* (1999). Ataxia in prion protein (PrP)-deficient mice is associated with upregulation of the novel PrP-like protein doppel. *J. Mol. Biol.* **292**, 797–817.
12. Zahn, R., von Schroetter, C. & Wüthrich, K. (1997). Human prion proteins expressed in *Escherichia coli*

and purified by high-affinity column refolding. *FEBS Letters*, **417**, 400–404.
13. Bax, A. & Grzesiek, S. (1993). Methodological advances in protein NMR. *Acc. Chem. Res.* **26**, 131–138.
14. Wüthrich, K. (1986). *NMR of Proteins and Nucleic Acids*, Wiley, New York.
15. Marion, D., Kay, L. E., Sparks, S. E., Torchia, D. A. & Bax, A. (1989). Three-dimensional heteronuclear NMR of ^{15}N-labelled proteins. *J. Am. Chem. Soc.* **111**, 1515–1517.
16. Güntert, P., Billeter, M., Ohlenschläger, O., Brown, L. R. & Wüthrich, K. (1998). Conformational analysis of protein and nucleic acid fragments with the new grid search algorithm FOUND. *J. Biomol. NMR*, **12**, 543–548.
17. Güntert, P., Mumenthaler, C. & Wüthrich, K. (1997). Torsion angle dynamics for NMR structure calculation with the new program DYANA. *J. Mol. Biol.* **273**, 283–298.
18. Wishart, D. S., Bigam, C. G., Holm, A., Hodges, R. S. & Sykes, B. D. (1995). ^{1}H, ^{13}C and ^{15}N random coil NMR chemical shifts of the common amino acids. I. Investigations of nearest-neighbor effects. *J. Biomol. NMR*, **5**, 67–81.
19. Herrmann, T., Güntert, P. & Wüthrich, K. (2002). Protein NMR structure determination with automated NOE assignment using the new software CANDID and the torsion angle dynamics algorithm DYANA. *J. Mol. Biol.* **319**, 209–227.
20. Luginbühl, P., Szyperski, T. & Wüthrich, K. (1995). Statistical basis for the use of $^{13}C^{\alpha}$ chemical shifts in protein structure determination. *J. Magn. Reson. B*, **109**, 229–233.
21. Williamson, M. P., Havel, T. F. & Wüthrich, K. (1985). Solution conformation of proteinase inhibitor IIA from bull seminal plasma by ^{1}H nuclear magnetic resonance and distance geometry. *J. Mol. Biol.* **182**, 295–315.
22. Luginbühl, P., Güntert, P., Billeter, M. & Wüthrich, K. (1996). The new program OPAL for molecular dynamics simulations and energy refinements of biological macromolecules. *J. Biomol. NMR*, **8**, 136–146.
23. Koradi, R., Billeter, M. & Güntert, P. (2000). Point-centered domain decomposition for parallel molecular dynamics simulation. *Comput. Phys. Commun.* **124**, 139–147.
24. Spera, S. & Bax, A. (1991). Empirical correlation between protein backbone conformation and C^{α} and C^{β} ^{13}C nuclear magnetic resonance shifts. *J. Am. Chem. Soc.* **113**, 5490–5492.
25. Wishart, D. S. & Sykes, B. D. (1994). The ^{13}C chemical-shift index: a simple method for the identification of protein secondary structure using ^{13}C chemical-shift data. *J. Biomol. NMR*, **4**, 171–180.
26. Wüthrich, K. (1994). NMR assignment as a basis for structural characterization of denatured states of globular proteins. *Curr. Opin. Struct. Biol.* **4**, 93–99.
27. Mo, H., Moore, R. C., Cohen, F. E., Westaway, D., Prusiner, S. B., Wright, P. E. & Dyson, H. J. (2001). Two different neurodegenerative diseases caused by proteins with similar structures. *Proc. Natl Acad. Sci. USA*, **98**, 2352–2357.
28. Prusiner, S. B., Groth, D. F., Bolton, D. C., Kent, S. B. & Hood, L. E. (1984). Purification and structural studies of a major scrapie prion protein. *Cell*, **38**, 127–134.
29. Behrens, A., Brandner, S., Genoud, N. & Aguzzi, A. (2001). Normal neurogenesis and scrapie pathogenesis in neural grafts lacking the prion protein homologue Doppel. *EMBO Rep.* **2**, 347–352.
30. Tuzi, N. L., Gall, E., Melton, D. & Manson, J. C. (2002). Expression of doppel in the CNS of mice does not modulate transmissible spongiform encephalopathy disease. *J. Gen. Virol.* **83**, 705–711.
31. Boelens, R., Burgering, M., Fogh, R. H. & Kaptein, R. (1994). Time-saving methods for heteronuclear multidimensional NMR of (^{13}C, ^{15}N) doubly labeled proteins. *J. Biomol. NMR*, **4**, 201–213.
32. Ikura, M., Kay, L. E., Tschudin, R. & Bax, A. (1990). Three-dimensional NOESY-HMQC spectroscopy of a ^{13}C-labelled protein. *J. Magn. Reson.* **86**, 204–209.
33. Güntert, P., Dötsch, V., Wider, G. & Wüthrich, K. (1992). Processing of multidimensional NMR data with the new software PROSA. *J. Biomol. NMR*, **2**, 619–629.
34. Farrow, N. A., Zhang, O., Forman-Kay, J. D. & Kay, L. E. (1994). A heteronuclear correlation experiment for simultaneous determination of ^{15}N longitudinal decay and chemical exchange rates of systems in slow equilibrium. *J. Biomol. NMR*, **4**, 727–734.
35. Bartels, C., Xia, T. H., Billeter, M., Güntert, P. & Wüthrich, K. (1995). The program XEASY for computer-supported NMR spectral analysis of biological macromolecules. *J. Biomol. NMR*, **6**, 1–10.
36. Nilges, M., Macias, M. J., O'Donoghue, S. I. & Oschkinat, H. (1997). Automated NOESY interpretation with ambiguous distance restraints: the refined NMR solution structure of the pleckstrin homology domain from β-spectrin. *J. Mol. Biol.* **269**, 408–422.
37. Folmer, R. H., Hilbers, C. W., Konings, R. N. & Nilges, M. (1997). Floating stereospecific assignment revisited: application to an 18 kDa protein and comparison with *J*-coupling data. *J. Biomol. NMR*, **9**, 245–258.
38. Cornell, W. D., Cieplak, P., Bayly, C. I., Gould, I. R., Merz, K. M., Jr, Ferguson, D. M. *et al.* (1995). A second generation force field for the simulation of proteins, nucleic acids, and organic molecules. *J. Am. Chem. Soc.* **117**, 5179–5197.
39. Koradi, R., Billeter, M. & Wüthrich, K. (1996). MOLMOL: a program for display and analysis of macromolecular structures. *J. Mol. Graph.* **14**, 51–55.
40. Billeter, M., Kline, A. D., Braun, W., Huber, R. & Wüthrich, K. (1989). Comparison of the high-resolution structures of the α-amylase inhibitor Tendamistat determined by nuclear magnetic resonance in solution and by X-ray diffraction in single crystals. *J. Mol. Biol.* **206**, 677–687.
41. Richarz, R. & Wüthrich, K. (1978). High-field ^{13}C nuclear magnetic resonance studies at 90.5 MHz of the basic pancreatic trypsin inhibitor. *Biochemistry*, **17**, 2263–2269.

Edited by M. F. Summers

(Received 28 August 2002; received in revised form 13 November 2002; accepted 14 November 2002)